Hindawi
Advances in Materials Science and Engineering
Volume 2018, Article ID 3750742, 10 pages
https://doi.org/10.1155/2018/3750742

Research Article

Effects of Zinc Oxide Nanoparticles on Properties of SAC0307 Lead-Free Solder Paste

Kannachai Kanlayasiri and Nadee Meesathien

Department of Industrial Engineering, Faculty of Engineering, King Mongkut's Institute of Technology Ladkrabang, Bangkok 10520, Thailand

Correspondence should be addressed to Kannachai Kanlayasiri; kkkannac@kmitl.ac.th

Received 26 February 2018; Revised 30 April 2018; Accepted 29 May 2018; Published 26 June 2018

Academic Editor: Michael Aizenshtein

This research investigates the effects of zinc oxide (ZnO) nanoparticles of varying concentrations 0.0, 0.25, 0.50, 0.75, and 1.0 wt.% on the melting temperatures, wettability, printability, slump, and interfacial microstructure of the ZnO-doped Sn-0.3Ag-0.7Cu lead-free solder pastes on the copper substrate. The results revealed that the introduction of the ZnO particles had no effect on the solidus and liquidus temperatures of the solders. The maximum wettability was achieved with 0.25 wt.% ZnO nanoparticles, while the printability was inversely correlated with the nano-ZnO concentrations. The findings also indicated that, at room temperature, the slumping and the nano-ZnO concentrations were positively correlated and that, under the 150°C thermal condition, the maximum slumping was achieved with 0.25 wt.% ZnO. The slumping mechanism of the SAC0307-xZnO solder pastes is also provided herein. Moreover, the experiments showed that Cu_6Sn_5 was the single intermetallic compound present in the interfacial layer between the solders and the copper substrate, with the maximum intermetallic layer thickness realized at the 0.25 wt.% ZnO concentration.

1. Introduction

Recent decades have witnessed a growing number of countries around the globe rigorously regulating the use of certain toxic substances in electronic products. Effective over a decade ago, the European Union's Restriction of Hazardous Substances (RoHS) directive restricts the use of six hazardous materials in the manufacture of various types of electronic and electrical equipment, including lead (Pb), mercury (Hg), cadmium (Cd), hexavalent chromium (Cr^{6+}), polybrominated biphenyls (PBB), and polybrominated diphenyl ether (PBDE) [1]. To comply with the RoHS directive, a variety of lead-free solders have thus been developed to replace the lead-bearing solders. In fact, the most commonly used lead-free solders belong to the Sn-Ag-Cu (SAC) group because of their functional electrical and mechanical properties [2].

By comparison, Sn-0.3Ag-0.7Cu (SAC0307) solder is a low-Ag SAC solder that is of lower cost and less Ag_3Sn in the solder matrix [3, 4]. The SAC0307 and other SAC solders nevertheless are plagued with low fatigue strength and creep resistance [5–8]. To mitigate, certain small particles were introduced into the solder to transform it into a composite material such that the movement of dislocations and the grain boundary slidings were hindered [6, 7, 9]. Importantly, with the advancement in the nanotechnology, many new nanoparticles have been synthesized and used as the dispersed phases in the solders (i.e., the nanocomposite solders) to enhance their mechanical properties [10]. However, the improvement in the fatigue strength and creep resistance comes with the alteration of the other properties of the solder, such as wettability and microstructure [11–19].

Moreover, in the case of solder paste, printability and slump are the additional characteristics required for further investigations [20–24]. Although the slump of solder paste is very critical to the formation of solder bridges leading to the failure of the circuit, the slumping mechanism has not been reported in the literature.

Zinc oxide (ZnO) nanoparticles are used as dispersed phase in nanocomposite solders to improve the properties of the solders [25–30]. Specifically, ZnO nanoparticles could improve the solder mechanical properties, including yield strength, tensile strength, and microhardness through microstructure refinement and dispersion strengthening [26–28]. In addition, the shear strength of solder joints could be enhanced with ZnO nanoparticles [28]. ZnO nanoparticles also suppressed the growth of intermetallic compounds during soldering, for example, Cu_6Sn_5 and Ag_3Sn [25, 29, 30].

This research investigates the effects of the ZnO nanoparticles of variable concentrations (i.e., 0.0, 0.25, 0.50, 0.75, and 1.0 wt.%) on the melting temperatures, wettability, printability, slump, and interfacial microstructure of the SAC0307-xZnO solder pastes on the copper substrate. The slumping mechanism is also provided herein.

2. Materials and Methods

In this research, the SAC0307 solder paste and the ZnO nanoparticles were used as the matrix and dispersed phases of the nanocomposite solder, respectively. The SAC0307 solder paste was prepared from the Sn-0.3Ag-0.7Cu solder paste (Nihon Almit) with the metallic particle sizes of 20–38 μm. The solder's melting temperature, density, and viscosity were 217–227°C, 4.16 g/cm^3, and 150–300 Pa·s, respectively. Meanwhile, the concentrations of the ZnO nanoparticles (SAC0307-xZnO; NanoMaterials Technology) in the solder paste were varied between 0.0, 0.25, 0.50, 0.75, and 1.0 wt.%. The nano-ZnO particle size, the melting temperature, and the density were 20–40 nm, 1970°C, and 5.61 g/cm^3. Moreover, the solder paste and the ZnO nanoparticles were mechanically mixed for 30 min for uniform mixture.

The melting (solidus and liquidus) temperatures of the SAC0307-xZnO solder pastes were determined using the differential scanning calorimetry technique (Netzsch DSC 204 F1 Phoenix) under the N_2 atmosphere and 10°C/min heating rate condition. In addition, the SAC0307-xZnO solder pastes were individually screened on a copper substrate according to the JIS Z3198-3:2003 standard and then reflow-soldered in an LPKF reflow oven with the reflow profile as per the JEDEC J-STD-020D.1 standard. The preheat temperature and time were 180°C and 80 s, while the reflow temperature, reflow time, and cool down time were 267°C, 210 s, and 60 s. The wettability, printability, slump, and intermetallic layer were subsequently examined and compared. In this research, the copper substrate was prepared from an oxygen-free high conductivity (OFHC) copper sheet with a thickness and surface roughness (R_a) of 0.35 mm and 0.06 μm. The wettability was assessed in terms of contact angle (θ), as shown in Figure 1 and (1):

$$\theta = \sin^{-1}\frac{2}{((A/h)+(h/A))}. \quad (1)$$

The printability is the ratio of the actual volume of solder paste on the substrate to the ideal volume of solder paste on the substrate [31]. The printability (P%) can be calculated by (2), where V_1 is the actual volume of the solder paste and V_0 is the ideal volume of the solder paste:

$$P\% = \frac{V_1}{V_0} \times 100\%. \quad (2)$$

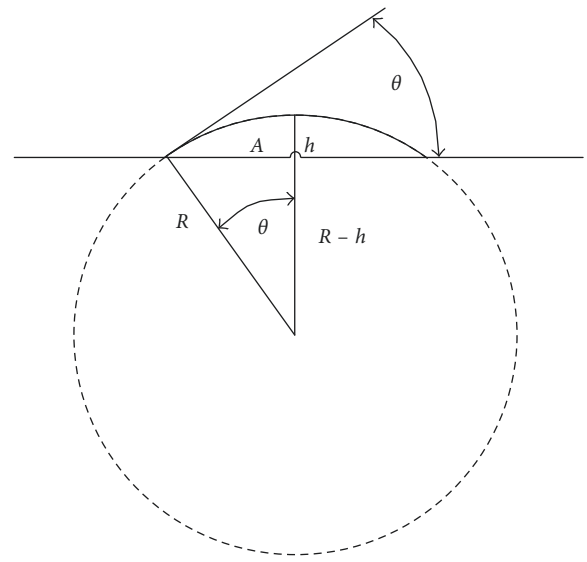

Figure 1: Contact angle measurement.

The slump testing was undertaken under two thermal conditions in accordance with the IPC-TM-650 testing procedure, each for 30 min: 25°C (at room temperature) and 150°C. The higher temperature testing (150°C) was carried out using a Memmert hot air oven. The slump (S_L%) could be calculated by (3), where D_s is the diameter of the stencil and D_p is the diameter of the pattern [32]:

$$S_L\% = \frac{D_s - D_p}{2} \times 100\%. \quad (3)$$

Furthermore, the reflowed solder joints were sectioned and the interfacial microstructure examined using the Bruker XRD model D8-Discover and Hitachi field emission scanning electron microscope (FE-SEM) coupled with IXRF Systems energy dispersive X-ray spectroscopy (EDS) to characterize the intermetallic layer. In this research, Image Pro® Express was used to determine the area and length of the intermetallic layer, and the intermetallic layer thickness was calculated by dividing the area of the intermetallic layer by its length. The reported thickness was the average thickness of three specimens of identical ZnO concentrations.

3. Results and Discussion

3.1. Melting Temperatures. Figure 2 illustrates the solidus and liquidus temperatures of the SAC0307-xZnO solder pastes at variable nano-ZnO concentrations (0.0, 0.25, 0.50, 0.75, and 1.0 wt.%). The initial solidus temperature and liquidus temperature of the SAC0307 solder (0.0 wt.% ZnO) were 216.6 and 231.2°C and remained relatively unchanged despite the incremental nano-ZnO concentrations,

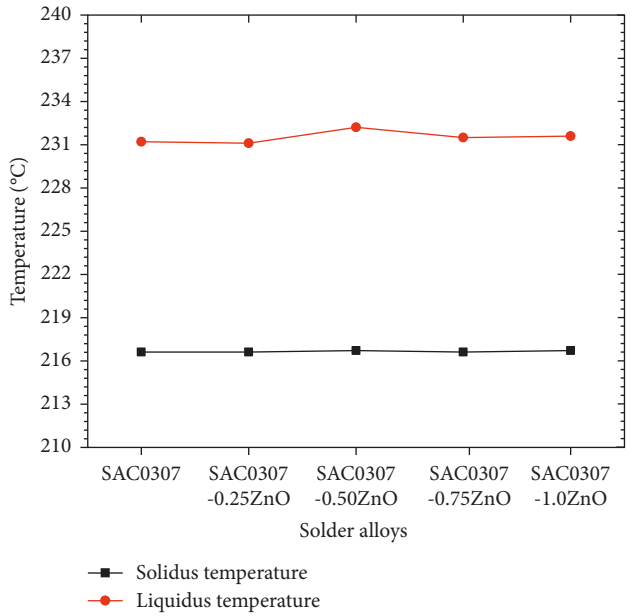

Figure 2: The solidus and liquidus temperatures of the SAC0307-xZnO solders at variable nano-ZnO concentrations.

indicating that the ZnO nanoparticles exerted negligible influence on the SAC0307-xZnO solidus and liquidus temperatures. The finding could be explained by Lindemann's melting theory, in which the solidus and liquidus temperatures of a single material are the inherent properties that are dependent on the interatomic distance and the root mean vibration amplitude [33]. It could thus be extrapolated that the presence of the ZnO nanoparticles neither alters the aforementioned parameters nor reacts with the solder. In other words, the introduction of the ZnO nanoparticles had no effect on the solidus and liquidus temperatures of the SAC0307-xZnO solder pastes.

3.2. Wettability on the Copper Substrate. The wettability of SAC0307-xZnO solders on the copper substrate was measured in terms of contact angle. In Figure 3, the contact angle of the initial SAC0307 solder was $22.24 \pm 0.61^{\circ}$ and became drastically smaller with 0.25 wt.% ZnO nanoparticles. The trend was nevertheless reversed as the nano-ZnO concentrations increased. The phenomenon could be attributed to the reduced surface tensions of the molten solder in the presence of ZnO nanoparticles in which the liquid-solid and liquid-vapor surface tensions decreased [34]. Meanwhile, the higher nano-ZnO concentrations elevated the viscosity of the molten solder, resulting in the upsurge in the contact angle [35–38]. The finding suggested that the solder contact angles could be manipulated by varying the nano-ZnO concentrations. With 0.25 wt.% ZnO nanoparticles, the contact angle decreased dramatically before gradually increasing with increase in ZnO. Given the minimum surface tensions, 0.25 wt.% was thus the optimal ZnO concentration. Meanwhile, excessive fractions of ZnO nanoparticles did not reduce the surface tensions but increased the viscosity of the molten solder.

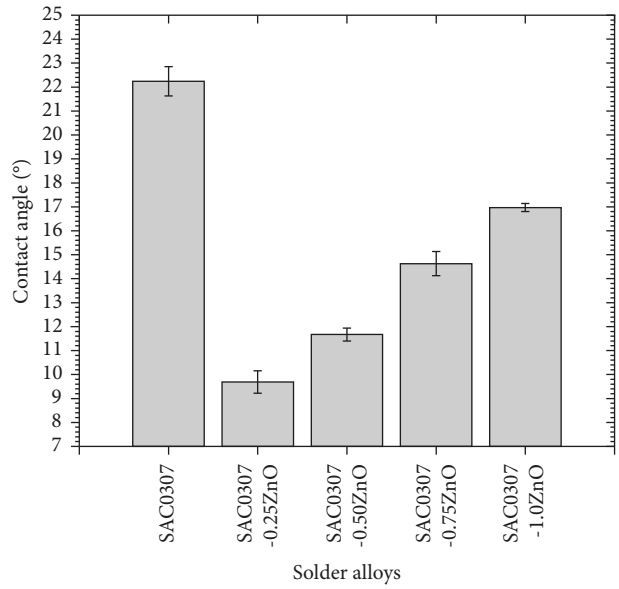

Figure 3: The contact angles of the SAC0307-xZnO solders on the copper substrate.

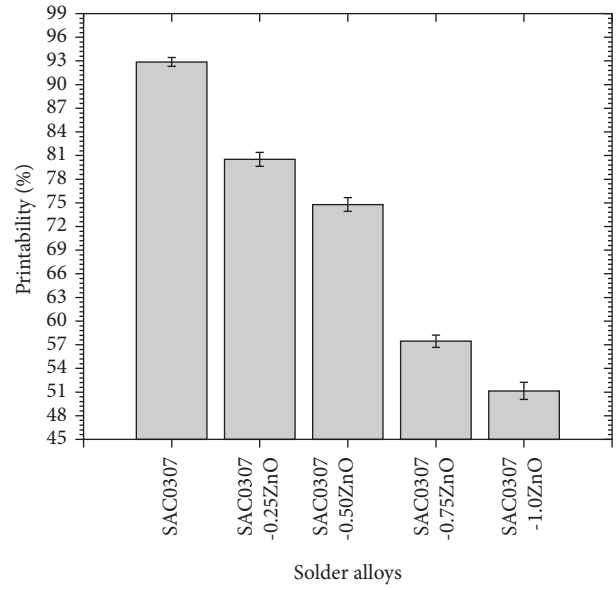

Figure 4: The printability of the SAC0307-xZnO solders on the copper substrate.

Interestingly, the low ZnO concentrations (0.0–0.25 wt.%) warrant further investigation to establish the relationship between the contact angle and ZnO concentrations.

3.3. Printability on the Copper Substrate. In Figure 4, the printability of the SAC0307 solder paste on the copper substrate was 92.87 ± 0.56 % and steadily decreased as the nano-ZnO concentrations increased. Specifically, the ZnO concentrations were inversely correlated with the printability of the solder paste on the copper substrate. This is because the higher ZnO concentrations caused the solder paste to become more viscous. The stickier solder paste in

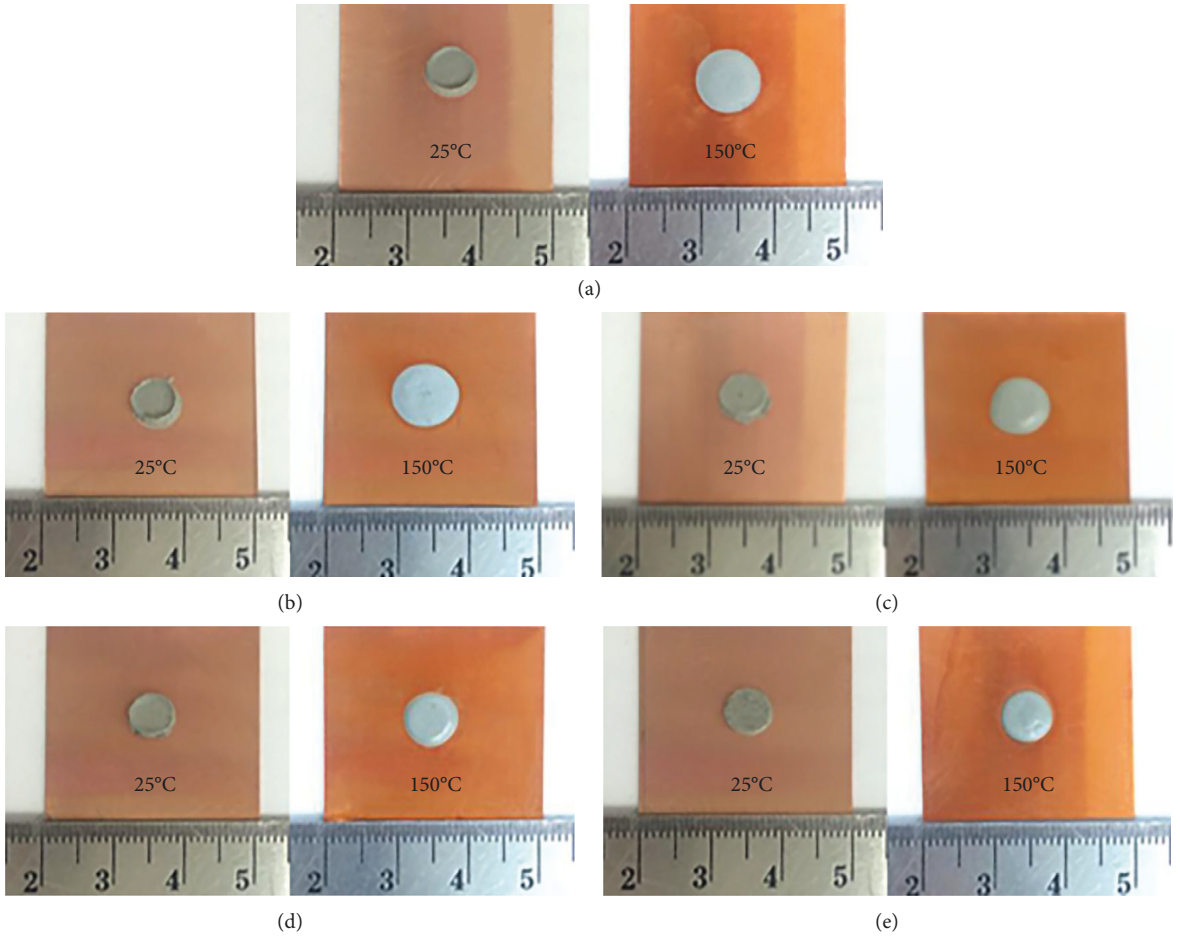

Figure 5: The slumping of the SAC0307-xZnO solders on the copper substrate: (a) SAC0307, (b) SAC0307-0.25ZnO, (c) SAC0307-0.50ZnO, (d) SAC0307-0.75ZnO, and (e) SAC0307-1.0ZnO.

turn contributed to excessive solder paste residues clinging to the stencil and the subsequent lower printability.

3.4. Slumping on the Copper Substrate. The slump testing of the experimental SAC0307-xZnO solder pastes on the copper substrate was carried out at room temperature (25°C) and at 150°C for 30 min each. Figure 5 shows the experimental results of slumping tests of SAC0307-xZnO solder pastes at both testing temperatures. Figure 6 illustrates the slumping results at room temperature, in which the initial slumping associated with the SAC0307 solder paste was 12.17 ± 0.76 % and increased with the increase in the nano-ZnO concentrations. Specifically, the solder became more susceptible to collapse and its diameter larger as the nano-ZnO concentrations rose.

The finding was attributable to the absorption of the moisture or liquid in the solder paste by the ZnO nanoparticles because the absorbed moisture or surrounding liquid lowers interparticle friction [39]. As a result, the nanoparticles became more free-flowing and less coalescent with other particles. Given that the amount of moisture or

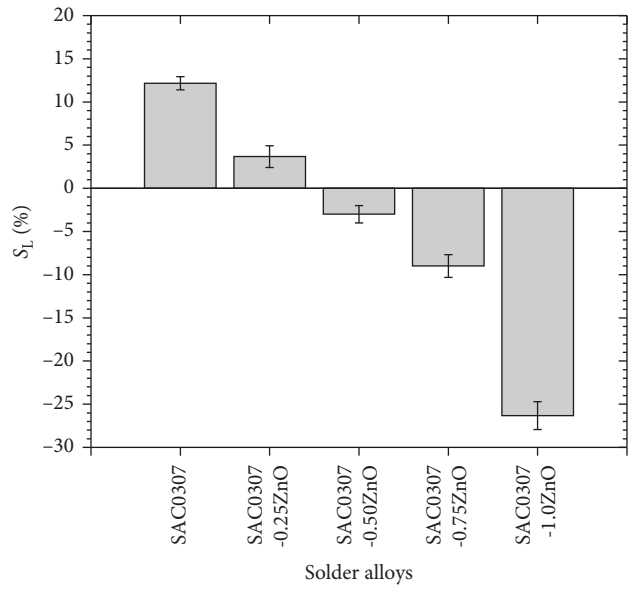

Figure 6: The slumping of the SAC0307-xZnO solders on the copper substrate at room temperature.

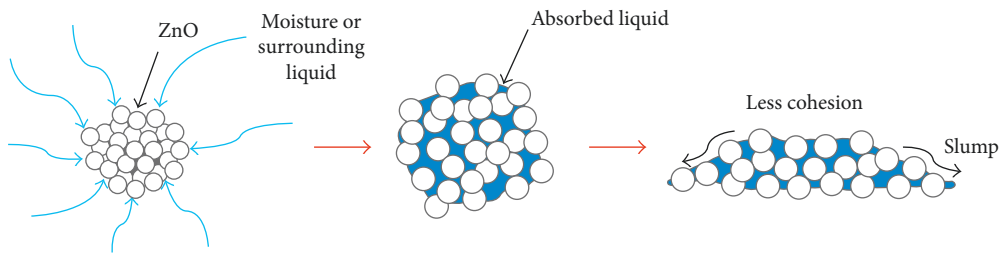

Figure 7: Slumping mechanism of the SAC0307-xZnO solders at room temperature.

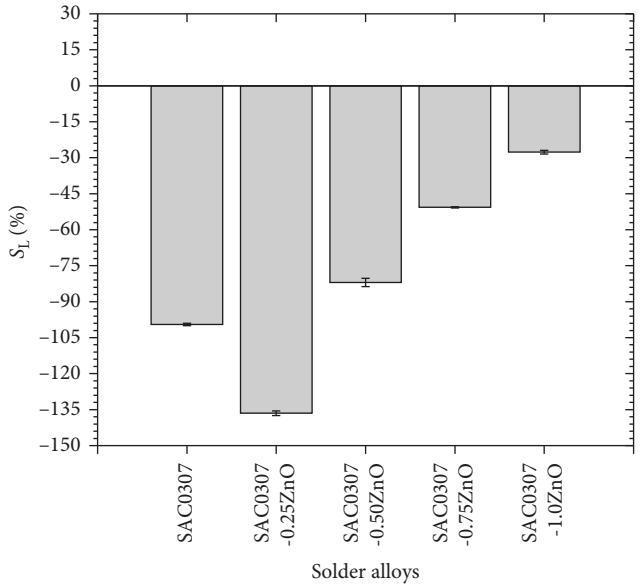

Figure 8: The slumping of the SAC0307-xZnO solders on the copper substrate at 150°C.

liquid was sufficient, the solder continued to collapse providing the greater slump as the nano-ZnO concentration increased. Figure 7 depicts the slumping mechanism of the SAC0307-xZnO solders on the copper substrate at room temperature.

Under the 150°C thermal condition, the slumping of the SAC0307-xZnO solders was greater than that at room temperature. In Figure 8, the initial slumping associated with the SAC0307 solder paste was $-99.50 \pm 0.50\%$ and increased to $\pm 136.50 \pm 1.00\%$ with 0.25 wt.% ZnO nanoparticles. The slumping trajectory was nevertheless reversed as the nano-ZnO increased.

In fact, with 0.25 wt.% ZnO, the slumping was greater than that of the SAC0307. The finding was attributable to, despite the evaporation, the sufficiently large amounts of remaining liquid in the solders which allow for the free-flowing of the low-concentration nanoparticles and the subsequent larger slump. The slumping however became smaller as the nano-ZnO concentrations increased. This was due to the liquid bridge phenomenon.

Unlike the slumping mechanism at room temperature (Figure 7), the slumping behavior under the 150°C condition was characterized by the evaporation of liquid in the solder paste. Given the evaporation and the higher nano-ZnO concentrations, the proportion of liquid to particles decreased and

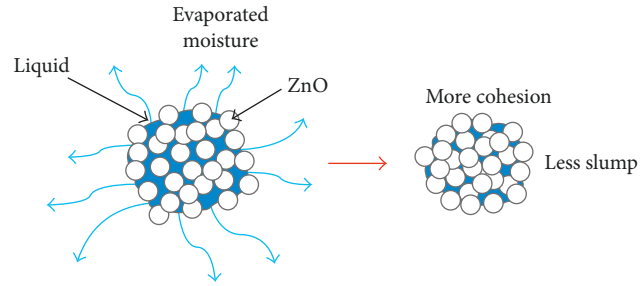

Figure 9: Slumping mechanism of the SAC0307-xZnO solders at 150°C.

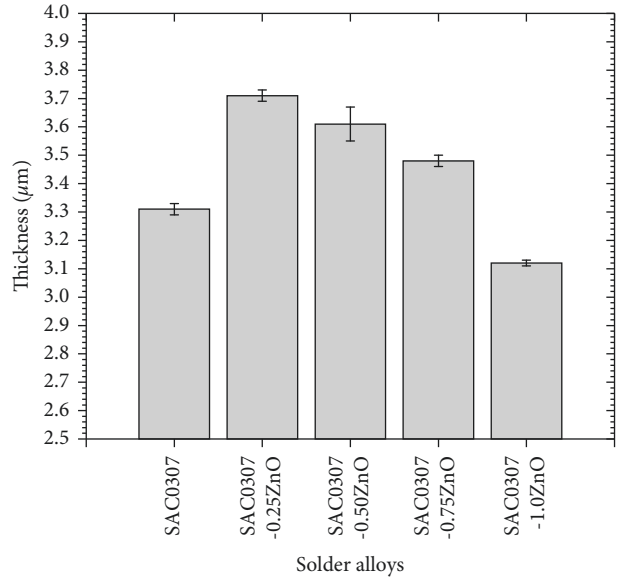

Figure 10: Thickness of Cu_6Sn_5 between the SAC0307-xZnO and the copper substrate.

the solder pastes were transformed from droplet or capillary state to funicular or pendular state. The funicular or pendular state solder pastes exhibited the greater attractive forces between particles [40], resulting in less slumping. Figure 9 illustrates the slumping mechanism of the SAC0307-xZnO solders on the copper substrate at 150°C.

3.5. Interfacial Layer. The interfacial layer between the SAC0307-xZnO solders and the copper substrate was of Cu_6Sn_5 intermetallic compound of varying thicknesses.

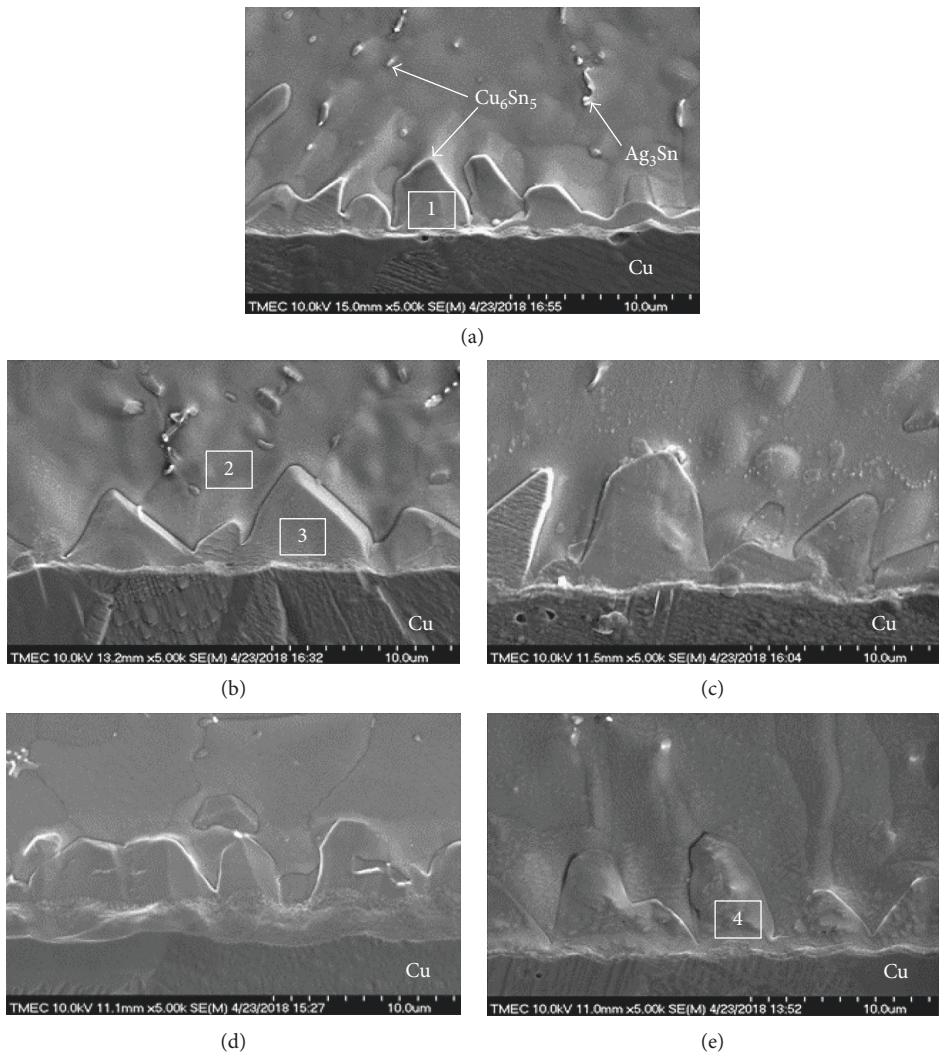

Figure 11: The intermetallic layer between the Cu substrate and (a) SAC0307, (b) SAC0307-0.25ZnO, (c) SAC0307-0.50ZnO, (d) SAC0307-0.75ZnO, and (e) SAC0307-1.00ZnO.

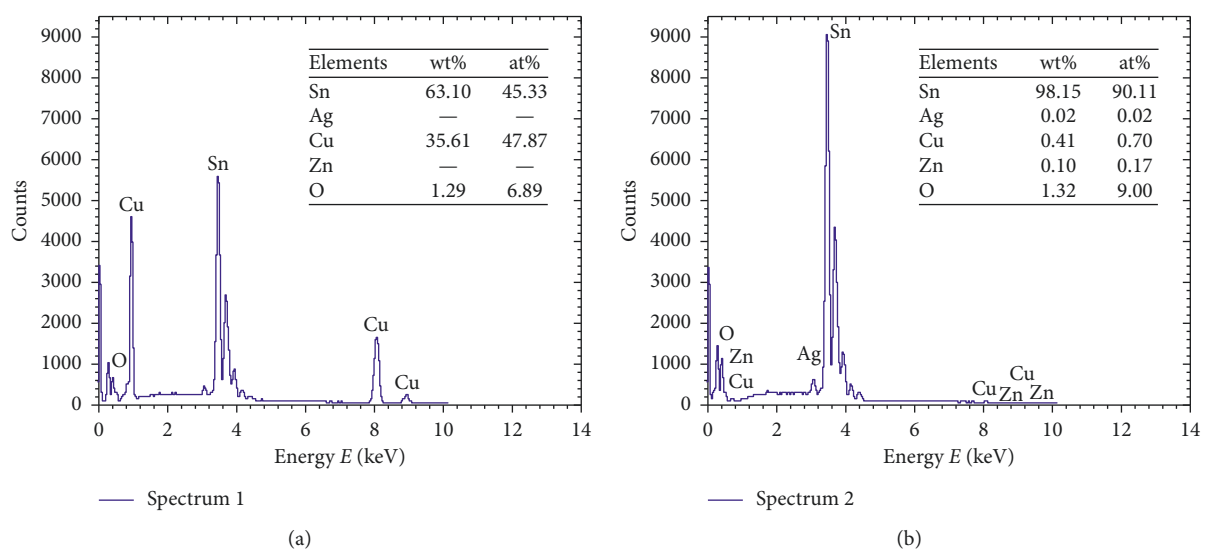

Figure 12: Continued.

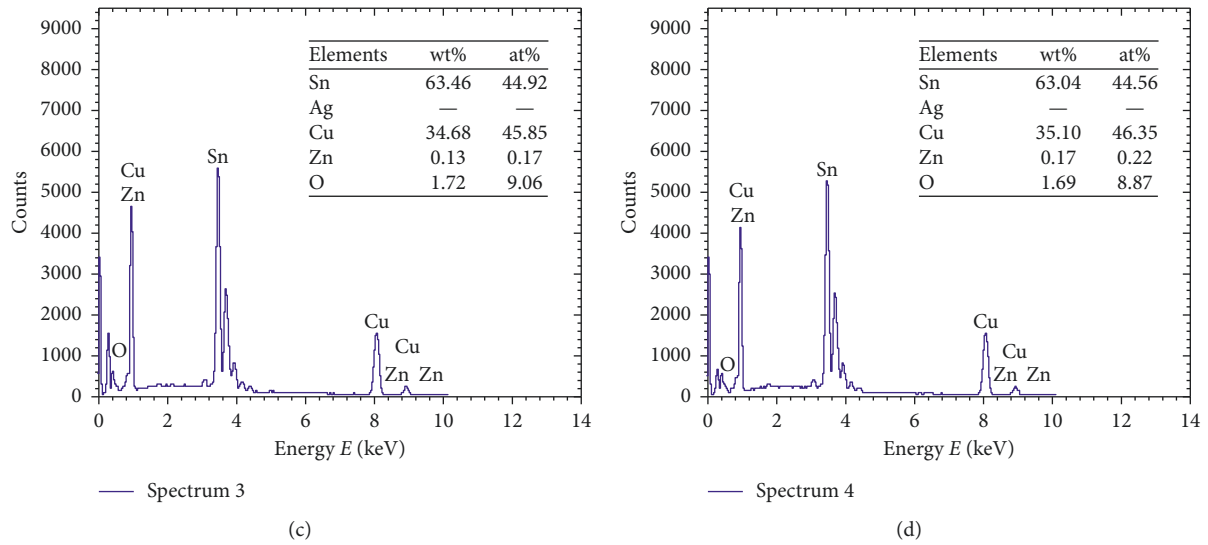

Figure 12: The EDS analysis of (a) Spectrum 1, (b) Spectrum 2, (c) Spectrum 3, and (d) Spectrum 4 of Figure 11.

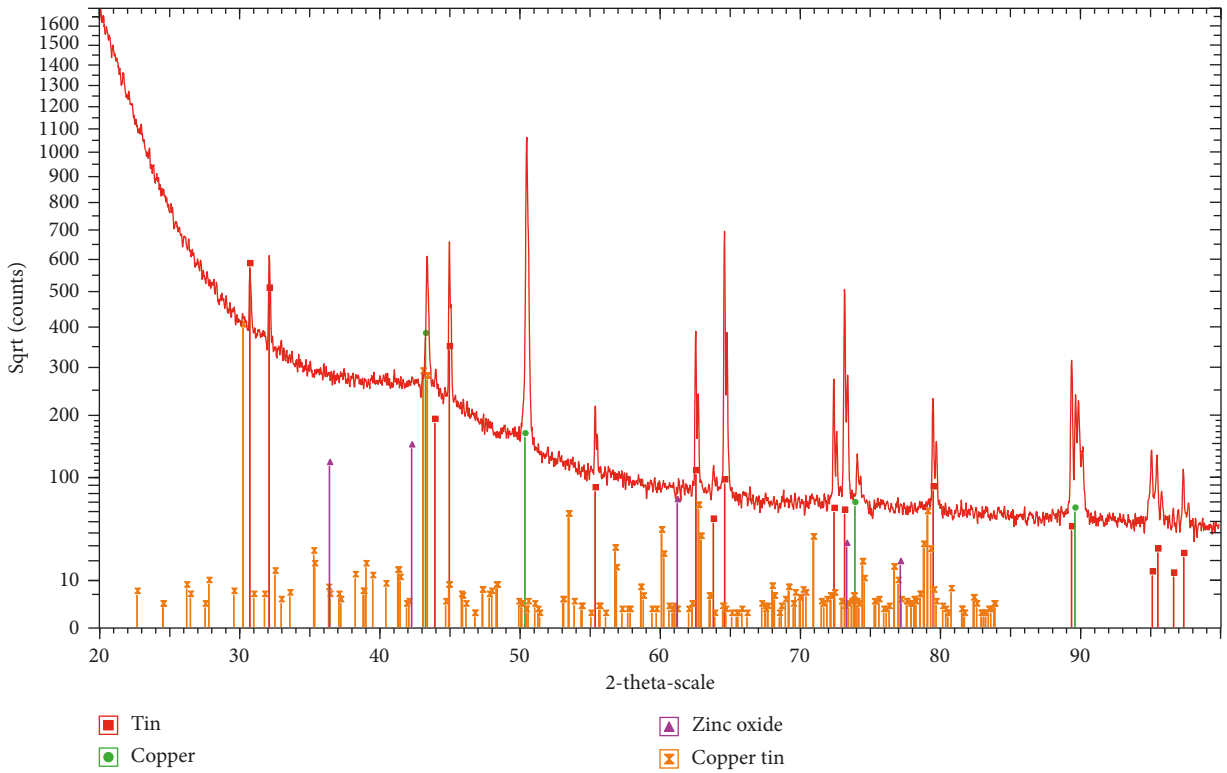

Figure 13: The XRD pattern of SAC0307-1.00ZnO.

Figure 10 compares the intermetallic layer thicknesses at the various nano-ZnO concentrations. The intermetallic layer thickness of the SAC0307 solder was $3.31 \pm 0.20\,\mu$m and increased with the introduction of 0.25 wt.% ZnO nanoparticles but then decreased as the nano-ZnO concentrations increased. However, the difference in the thicknesses was marginal among the SAC0307-xZnO solders. Figures 11(a) and 11(b) compare the intermetallic layers associated with SAC0307 and SAC0307-1.0ZnO solders on the copper substrate.

The increased thickness of the Cu_6Sn_5 layer was attributable to the ZnO nanoparticles acting as the new nucleation sites for the formation of intermetallic phase, resulting in a thicker Cu_6Sn_5 layer, consistent with Peng et al. [28] and Xing et al. [41]. However, at higher nano-ZnO concentrations, the Cu_6Sn_5 layer thickness decreased. This was attributable to the nanoparticles, despite acting as the nucleation sites, restricting the growth of the intermetallic compound by lowering the surface energy. From the adsorption theory [34], the surface energy of Cu_6Sn_5 crystal can be written as follows:

$$\sum_k \left(\gamma_c^k A_k\right) = \sum_k \left(\gamma_0^k - RT \int_0^c \frac{\Gamma^k}{c}\, dc\right) A_k, \quad (4)$$

where γ_c^k is the surface energy per unit area of the kth crystal plane of Cu_6Sn_5 with the adsorption of ZnO nanoparticles, A_k is the area of the kth crystal plane, γ_0^k is the surface energy per unit area of the kth crystal plane of Cu_6Sn_5 without the adsorption of ZnO nanoparticles, R is the gas constant, T is the absolute temperature, Γ^k is the amount of ZnO nanoparticles adsorbed per unit area of the kth crystal plane, and c is the total concentration of ZnO nanoparticles.

From (4), the surface energy of Cu_6Sn_5 is minimized when $(\sum_k (RT \int_0^c (\Gamma^k/c)\, dc) A_k)$ is maximized since $(\sum_k (\gamma_0^k) A_k)$ is constant (i.e., independent of the ZnO concentration). Therefore, the surface energy of Cu_6Sn_5 decreased with increase in the ZnO nanoparticles adsorbed on the crystal. The lower surface energy in turn contributed to inferior Cu_6Sn_5 grain growth. Although the nanoparticles acted as the nucleation sites, the reduced surface energy restricted the Cu_6Sn_5 layer thickness. This was more pronounced at higher nano-ZnO concentrations.

Figures 11 and 12 illustrate FE-SEM images and EDS analysis of the solder joints between SAC0307-xZnO and the copper substrate. The experimental results showed that Cu_6Sn_5 was the only intermetallic compound present in the scallop-shaped interfacial layer. The Cu_6Sn_5 intermetallic compound could be found at the interfacial zone and in the solder matrix, as shown in Figure 11(a). Ag_3Sn intermetallic phase was also present. Despite the ZnO nanoparticles, the nanoparticles were undetectable by FE-SEM; however, they were detected by EDS and XRD in the intermetallic layer and the solder matrix (Figures 12(a)–12(d) and 13). The retained ZnO nanoparticles were positively correlated to the Zn concentration. Zn in the intermetallic layer and the solder matrix increased (i.e., 0.10 to 0.17 wt.%) in response to the increase in ZnO doped into the solder paste. These numbers were the ZnO nanoparticles remaining in the solder paste following the expulsion during the reflow process [28].

4. Conclusions

This research investigated the effects of ZnO nanoparticles on the melting temperatures, wettability, printability, slump, and interfacial microstructure of the SAC0307-xZnO lead-free solder pastes on the copper substrate. The experimental results are summarized below:

(1) The addition of ZnO nanoparticles had no effect on the solidus and liquidus temperatures of the solders.

(2) The ZnO nanoparticles improved the wettability of the solder pastes, and the maximum wettability was achieved with 0.25 wt.% ZnO nanoparticles.

(3) The printability of the solders on the copper substrate decreased with increase in the nano-ZnO concentration.

(4) At room temperature, the slumping decreased with increase in the nano-ZnO concentration. Meanwhile, at 150°C, the maximum slumping was achieved with 0.25 wt.% ZnO concentration.

(5) The maximum thickness of Cu_6Sn_5 intermetallic layer was realized with 0.25 wt.% ZnO.

Data Availability

The data used to support the findings of this study are available from the corresponding author upon request.

Conflicts of Interest

The authors declare that there are no conflicts of interest regarding the publication of this paper.

Acknowledgments

This research was sponsored by the Higher Education Research Promotion and National Research University Project of Thailand, the Office of the Higher Education Commission.

References

[1] D. Shangguan, *Lead-Free Solder Interconnect Reliability*, ASM International, Materials Park, OH, USA, 2005.

[2] M. Abtew and G. Selvaduray, "Engineering lead-free solders in microelectronic," *Materials Science and Engineering R*, vol. 27, pp. 95–106, 2000.

[3] K. S. Kim, S. H. Huh, and K. Suganuma, "Effects of fourth alloying additive on microstructures and tensile properties of Sn-Ag-Cu alloy and joints with Cu," *Microelectronics Reliability*, vol. 43, no. 2, pp. 259–267, 2003.

[4] F. Sun, P. Hochstenbach, W. D. Van Driel, and G. Q. Zhang, "Fracture morphology and mechanism of IMC in low-Ag SAC Solder/UBM (Ni(P)-Au) for WLCSP," *Microelectronics Reliability*, vol. 48, no. 8-9, pp. 1167–1170, 2008.

[5] H. Conrad, Z. Guo, Y. Fahmy, and D. Yang, "Influence of microstructure size on the plastic deformation kinetics, fatigue crack growth rate, and low-cycle fatigue of solder joints," *Journal of Electronic Materials*, vol. 28, no. 9, pp. 1062–1070, 1999.

[6] J. L. Marshall, J. Calderon, J. Sees, G. Lucey, and J. S. Hwang, "Composite Solders," *IEEE Transactions on Components, Hybrids, and Manufacturing Technology*, vol. 14, no. 4, pp. 698–702, 1991.

[7] H. S. Betrabet, S. M. McGee, and J. K. McKinlay, "Processing dispersion-strengthened Sn-Pb solders to achieve microstructural refinement and stability," *Scripta Metallurgica et Materialia*, vol. 25, no. 10, pp. 2323–2328, 1991.

[8] H. Mavoori and S. Jin, "New, creep-resistant, low melting point solders with ultrafine oxide dispersions," *Journal of Electronic Materials*, vol. 27, no. 11, pp. 1216–1222, 1998.

[9] A. A. El-Daly, A. Fawzy, S. F. Mansour, and M. J. Younis, "Thermal analysis and mechanical properties of Sn-1.0Ag-0.5Cu solder alloy after modification with SiC nano-sized particles," *Journal of Materials Science: Materials in Electronics*, vol. 24, no. 8, pp. 2976–2988, 2013.

[10] J. Shen and Y. C. Chan, "Research advances in nano-composite solders," *Microelectronics Reliability*, vol. 49, no. 3, pp. 223–234, 2009.

[11] K. Bukat, J. Sitek, M. Koscielski et al., "SAC 305 solder paste with carbon nanotubes–part I: investigation of the influence of the carbon nanotubes on the SAC solder paste properties,"

Soldering & Surface Mount Technology, vol. 24, no. 4, pp. 267–279, 2012.

[12] M. Jakubowska, K. Bukat, M. Kościelski et al., "Investigation of properties of the SAC solder paste with the silver nanoparticle and carbon nanotube additives and the nano solder joints," in *Proceedings of the Electronics System Integration Technology Conference*, pp. 1–6, Berlin, Germany, September 2010.

[13] S. Y. Chang, C. C. Jain, T. H. Chuang, L. P. Feng, and L. C. Tsao, "Effect of addition of TiO_2 nanoparticles on the microstructure, microhardness and interfacial reactions of Sn3.5AgXCu solder," *Materials and Design*, vol. 32, no. 10, pp. 4720–4727, 2011.

[14] Y. Tang, G. Y. Li, D. Q. Chen, and Y. C. Pan, "Influence of TiO_2 nanoparticles on IMC growth in Sn-3.0Ag-0.5Cu-xTiO_2 solder joints during isothermal aging process," *Journal of Materials Science: Materials in Electronics*, vol. 25, no. 2, pp. 981–991, 2014.

[15] S. L. Tay, A. S. M. A. Haseeb, and M. R. Johan, "Addition of cobalt nanoparticles into Sn-3.8Ag-0.7Cu lead-free solder by paste mixing," *Soldering & Surface Mount Technology*, vol. 23, no. 1, pp. 10–14, 2011.

[16] L. C. Tsao, C. H. Huang, C. H. Chung, and R. S. Chen, "Influence of TiO_2 nanoparticles addition on the microstructural and mechanical properties of Sn0.7Cu nano-composite solder," *Materials Science and Engineering A*, vol. 545, pp. 194–200, 2012.

[17] L. C. Tsao, "An investigation of microstructure and mechanical properties of novel Sn3.5Ag0.5Cu–*X*TiO_2 composite solders as functions of alloy composition and cooling rate," *Materials Science and Engineering A*, vol. 529, pp. 41–48, 2011.

[18] L. C. Tsao, "Suppressing effect of 0.5 wt.% nano-TiO_2 addition into Sn–3.5Ag–0.5Cu solder alloy on the intermetallic growth with Cu substrate during isothermal aging," *Journal of Alloys and Compounds*, vol. 509, no. 33, pp. 8441–8448, 2011.

[19] D. C. Lin, S. Liu, T. M. Guo, G. X. Wang, T. S. Srivatsan, and M. Petraroli, "An investigation of nanoparticles addition on solidification kinetics and microstructure development of tin-lead solder," *Materials Science and Engineering A*, vol. 360, no. 1-2, pp. 285–292, 2003.

[20] R. R. Lathrop, "Solder paste print qualification using laser triangulation," *IEEE Transactions on Components, Packaging, and Manufacturing Technology: Part C*, vol. 20, no. 3, pp. 174–182, 1997.

[21] C. H. Chen, W. Wong, J. C. C. Lo, F. Song, and S. W. R. Lee, "Characterization and comparison of five SAC-based solder pastes for Pb-free reflow soldering," in *Proceedings of the International Symposium on High Density Packaging and Microsystem Integration*, Shanghai, China, June 2007.

[22] A. Araźna, G. Kozioł, W. Stęplewski, and J. Borecki, "Assessment of lead-free solder pastes with different type of powder for fine-pitch application," in *in Proceedings of the 31st International Spring Seminar on Electronics Technology*, pp. 579–584, Budapest, Hungary, May 2008.

[23] B. An and Y. Wu, "Evaluating the printability of solder paste from paste roll characteristics," in *Proceedings of the 11th International Conference on Electronic Packaging Technology & High Density Packaging*, pp. 1186–1189, Xi'an, China, August 2010.

[24] K. Li, Y. Lei, J. Lin, B. Liu, H. Bai, and J. Qin, "Development of Sn-Bi systems lead-free solder paste," in *Proceedings of the 14th International Conference on Electronic Packaging Technology*, pp. 160–162, Dalian, China, August 2013.

[25] A. Fawzy, S. A. Fayek, M. Sobhy, E. Nassr, M. M. Mousa, and G. Saad, "Effect of ZnO nanoparticles addition on thermal, microstructure and tensile properties of Sn-3.5Ag-0.5 Cu (SAC355) solder alloy," *Journal of Materials Science: Materials in Electronics*, vol. 24, no. 9, pp. 3210–3218, 2013.

[26] A. A. El-Daly, T. A. Elmosalami, W. M. Desoky, M. G. El-Shaarawy, and A. M. Abdraboh, "Tensile deformation behavior and melting property of nano-sized ZnO particles reinforced Sn–3.0Ag–0.5Cu lead-free solder," *Materials Science and Engineering A*, vol. 618, pp. 389–397, 2014.

[27] A. N. Fouda and E. A. Eid, "Influence of ZnO nano-particles addition on thermal analysis, microstructure evolution and tensile behavior of Sn-5.0 wt% Sb-0.5 wt% Cu lead-free solder alloy," *Materials Science and Engineering A*, vol. 632, pp. 82–87, 2015.

[28] H. Peng, G. Chen, L. Mo, Y. C. Chan, F. Wu, and H. Liu, "An investigation on the ZnO retained ratio, microstructural evolution, and mechanical properties of ZnO doped Sn3.0Ag0.5Cu composite solder joints," *Journal of Materials Science: Materials in Electronics*, vol. 27, no. 9, pp. 9083–9093, 2016.

[29] A. E. Hammad and A. A. Ibrahiem, "Enhancing the microstructure and tensile creep resistance of Sn-3.0Ag-0.5Cu solder alloy by reinforcing nano-sized ZnO particles," *Microelectronics Reliability*, vol. 75, pp. 187–194, 2017.

[30] G. S. Al-Ganainy, A. A. El-Daly, A. Fawzy, and N. Hussein, "Effect of adding nanometric ZnO particles on thermal, microstructure and tensile creep properties of Sn–6.5 wt% Zn–3 wt% In solder alloy," *Journal of Materials Science: Materials in Electronics*, vol. 28, no. 18, pp. 13303–13312, 2017.

[31] E. H. Amalu, N. N. Ekere, and S. Mallik, "Evaluation of rheological properties of lead-free solder pastes and their relationship with transfer efficiency during stencil printing process," *Materials and Design*, vol. 32, no. 6, pp. 3189–3197, 2011.

[32] J. W. Evans, *A Guide to Lead-Free Solders: Physical Metallurgy and Reliability*, Springer, London, UK, 2007.

[33] F. Lindemann, "The calculation of molecular vibration frequencies," *Zeitschrift für Physik*, vol. 11, pp. 609–615, 1910.

[34] D. H. Jung, A. Sharma, D. U. Lim, J. H. Yun, and J. P. Jung, "Effects of AlN nanoparticles on the microstructure, solderability, and mechanical properties of Sn-Ag-Cu solder," *Metallurgical and Materials Transactions A: Physical Metallurgy and Materials Science*, vol. 48, no. 9, pp. 4372–4384, 2017.

[35] X. Liu, M. Huang, C. M. L. Wu, and L. Wang, "Effect of Y_2O_3 particles on microstructure formation and shear properties of Sn-58Bi solder," *Journal of Materials Science: Materials in Electronics*, vol. 21, no. 10, pp. 1046–1054, 2010.

[36] Y. Li, X. Zhao, Y. Liu, Y. Wang, and Y. Wang, "Effect of TiO_2 addition concentration on the wettability and intermetallic compounds growth of Sn3.0Ag0.5Cu-xTiO_2 nano-composite solders," *Journal of Materials Science: Materials in Electronics*, vol. 25, no. 9, pp. 3816–3827, 2014.

[37] A. Sharma, B. G. Baek, and J. P. Jung, "Influence of La_2O_3 nanoparticle additions on microstructure, wetting, and tensile characteristics of Sn-Ag-Cu alloy," *Materials and Design*, vol. 87, pp. 370–379, 2015.

[38] G. Chen, H. Peng, V. V. Silberschmidt, Y. C. Chan, C. Liu, and F. Wu, "Performance of Sn-3.0Ag-0.5Cu composite solder with TiC reinforcement: Physical properties, solderability and microstructural evolution under isothermal ageing," *Journal of Alloys and Compounds*, vol. 685, pp. 680–689, 2016.

[39] M. Rhodes, *Introduction to Particle Technology* Vol. 7, John Wiley & Sons, Hoboken, NJ, USA, 2nd edition, 2008.

[40] D. M. Newitt and J. M. Conway-Jones, "A contribution to the theory and practice of granulation," *Transactions of the Institution of Chemical Engineers*, vol. 36, pp. 422–442, 1958.

[41] W. Q. Xing, X. Y. Yu, H. Li et al., "Effect of nano Al_2O_3 additions on the interfacial behavior and mechanical properties of eutectic Sn-9Zn solder on low temperature wetting and soldering of 6061 aluminum alloys," *Journal of Alloys and Compounds*, vol. 695, pp. 574–582, 2017.